

High Resolution Calculations of Merging Neutron Stars III: Gamma-Ray Bursts

Stephan Rosswog¹, Enrico Ramirez-Ruiz² and Melvyn B. Davies¹

1. *Department of Physics and Astronomy, University of Leicester, LE1 7RH, Leicester, UK.*

2. *Institute of Astronomy, Madingley Road, Cambridge, CB3 0HA, UK.*

ABSTRACT

Recent three dimensional, high-resolution simulations of neutron star coalescences are analysed to assess whether short gamma-ray bursts (GRBs) could originate from such encounters. The two most popular modes of energy extraction – namely the annihilation of $\nu\bar{\nu}$ and magnetohydrodynamic processes – are explored in order to investigate their viability in launching GRBs. We find that $\nu\bar{\nu}$ annihilation can provide the necessary stresses to drive a highly relativistic expansion. But unless the outflow is beamed into less than one percent of the solid angle this mechanism may fail to explain the apparent isotropized energies implied for short GRBs at cosmological distances. We argue that the energetic, neutrino-driven wind that accompanies the merger event will have enough pressure to provide adequate collimation to the $\nu\bar{\nu}$ -annihilation-driven jet, thereby comfortably satisfying constraints on event rate and apparent luminosity. We also assess magnetic mechanisms to transform the available energy into a GRB. If the central object does not collapse immediately into a black hole it will be convective and it is expected to act as an effective large scale dynamo amplifying the seed magnetic fields to a few times 10^{17} G within a small fraction of a second. The associated spindown time scale is 0.2 s, coinciding with the typical duration of a short GRB. The efficiencies of the various assessed magnetic processes are high enough to produce isotropized luminosities in excess of 10^{52} ergs/s even without beaming.

Key words: dense matter; hydrodynamics; neutrinos; gamma rays: bursts; stars: neutron; methods: numerical

1 INTRODUCTION

The progenitors of gamma-ray bursts (GRBs) are not well identified. The current view of a majority of researchers is that GRBs arise in a very small fraction ($\sim 10^{-6}$) of stars which undergo a catastrophic energy release event towards the end of their evolution (see Mészáros 2002 for a recent review). Observationally (Kouveliotou et al. 1993) the short (< 2 s) and long (> 2 s) bursts appear to represent two distinct subclasses, and one early proposal to explain this was that accretion induced collapse of a white dwarf (WD) into a neutron star (NS) might be a candidate for the long bursts, while NS-NS mergers could provide the short ones (Katz & Canel 1996).

Observational studies related to the possible progenitors are restricted, so far, to the class of long duration bursts. For these bursts, the fading X-ray and optical afterglow emission is predominantly localized within the optical image of the host galaxy (Bloom et al. 2002). Several of these hosts show signs of ongoing star formation activity, necessary for the presence of young, massive progenitor stars. This is in disagreement with most predictions of the merger site of NS-NS binaries which suggest that high spatial velocities and long inspiral times would take these binaries, in more than half of the cases, outside of the confines of the host galaxy before they merge and produce a burst (Fryer, Woosley & Hart-

mann 1999; but see Belczynski, Bulik & Kalogera 2002). Moreover, theoretical estimates (e.g. Ruffert et al. 1997; Popham et al. 1998; Narayan et al. 1992, 2001; Rosswog & Davies 2002; Lee & Ramirez-Ruiz 2002) suggest that NS-NS and NS-BH mergers are only likely to produce bursts of the short category.

According to the above reasoning, there is a possible association between the type of GRB progenitor and the duration of the burst. Short GRBs may involve compact binaries that should occur predominantly in the low-density outskirts of the host galaxy while long GRBs are more likely associated with massive stars that, at the end of their evolution, are still within the high density cloud in which they formed (e.g. Woosley 1993; Chevalier & Li 1999; Ramirez-Ruiz et al. 2001). This picture of a long GRB as a death throes of a massive star is further corroborated by the observation of underlying supernovae in the afterglows of several bursts, so far most convincingly demonstrated for GRB030329 (Stanek et al. 2003).

Compact binaries are appealing candidates since they provide huge reservoirs of gravitational binding energy and, owing to centrifugal forces, a *baryon-clean* region will form naturally along the binary rotation axis. It is in this region where a sudden energy release is quickly and continuously transformed into a radiation dominated fluid with a high entropy per baryon (Cavallo & Rees

1978; Goodman 1986; Paczyński 1986; Shemi & Piran 1990; Piran 1999). In numerical simulations of such an event a high resolution of the outer debris layers is needed because even a tiny mass fraction in the outflow severely limits the attainable Lorentz factor – for instance, a fireball of $\sim 10^{53}$ erg would not be able to accelerate an outflow to $\Gamma \approx 100$ if loaded with more than $\sim 5 \times 10^{-4} M_{\odot}$. An $e^{\pm} - \gamma$ fireball arises from the enormous compressional heating and dissipation associated with the accretion – possibly involving $\nu\bar{\nu}$ annihilation or magnetic fields in excess of 10^{14} Gauss – which can in principle provide the driving stresses leading to relativistic expansion. Both modes of energy extraction from such binary encounters are discussed in this paper.

Global simulations of compact object mergers have been performed by various groups in order to assess their viability as possible GRB progenitors (Davies et al. 1994, Ruffert et al. 1996, 1997, 1999, 2001, Rosswog et al. 1999, 2000, 2002a, 2002b, Lee & Kluzniak 1999a, 1999b, Lee 2000, Lee 2001). So far it has only been possible to address the $\nu\bar{\nu}$ annihilation mechanism quantitatively (Jaroszynski 1993, Mochkovitch et al. 1993, Ruffert et al. 1997b, Popham et al. 1999, Ruffert & Janka 1999, Asano & Fukuyama 2000, 2001, Salmonson & Wilson 2001, Rosswog & Ramirez-Ruiz 2002). Simulations as to how magnetised, three dimensional flows close to nuclear density behave in strong gravitational fields are still to be done. The key to using simulations productively is to isolate questions that can realistically be addressed and where the outcome is unknown. The analysis of such simulations then can guide and inspire the way we think about the problem and the questions we pose.

In this paper, we report on the three-dimensional high-resolution merger simulations, which were done using a realistic equation of state and employing a detailed multi-flavour neutrino treatment. § 2 gives a short review of the physics and techniques used in the current model, followed by a concise summary of previous results. § 3 discusses the potential of $\nu\bar{\nu}$ annihilation as a viable source for GRB production and compares it with several magnetic GRB mechanisms. § 4 provides a detailed study of the distribution of merger sites with respect to their host galaxies. The summary and a discussion of the results are then presented in § 5.

2 BASIC MODEL FEATURES AND PREVIOUS RESULTS

We have performed a set of high-resolution simulations of the last inspiral stages and the final coalescence of a double neutron star system. Information regarding the numerical method, the initial conditions and the hydrodynamic evolution can be found in Rosswog & Davies (2002) hereafter referred to as paper I. A detailed account of the involved neutrino physics and its numerical treatment is presented in Rosswog & Liebendörfer 2003 (paper II). In the current paper we turn our attention to the viability of NS binary coalescences as central engines of GRBs, especially of those belonging to the short duration category.

The smoothed particle hydrodynamics method (SPH; e.g. Benz 1990 or Monaghan 1992) is used to solve the equations of hydrodynamics for the neutron star fluid. We have used a vastly improved artificial viscosity scheme (Rosswog et al. 2000) for these simulations with artificial viscosity being active only during shocks and being efficiently suppressed in pure shear flows (see paper I for a measurement of the effective α -viscosity in the simulations). We use a nuclear equation of state (EOS) for hot and dense nuclear matter. Our EOS is based on the tables provided by Shen et al. (1998a, 1998b), the lepton and photon contributions are included, and it is

extended smoothly to the low-density regime with a gas consisting of neutrons, alpha particles, electrons, positrons and photons. For details concerning the EOS we refer the reader to paper I. To account for cooling and changes in the electron fraction of the neutron star debris we have implemented a detailed multi-flavour neutrino treatment (paper II). We use a binary tree (Benz 1990b) to calculate the Newtonian self-gravity and add the back-reaction forces that emerge from the emission of gravitational waves.

We follow the system evolution starting at an initial separation of $\sim 3R_{ns}$, where R_{ns} is the radius of an isolated NS. The initial separation is comparable to the dynamical stability limit of the binary, so that the two neutron stars merge within a few milliseconds, and leave behind a differentially rotating, super massive ($\sim 2.5 M_{\odot}$) NS surrounded by dense, shock-heated debris. The differential rotation is expected to stabilise the central object efficiently against gravitational collapse. Although the time scale until collapse sets in is quite sensitive to the details of the merger, the remnant may remain stable for a time that is interesting for the production of a GRB (Rosswog & Ramirez-Ruiz 2002). The debris is heated initially via shocks (for example when two spiral arms merge supersonically, see Fig. 13 in paper I) and later via shear motion. The innermost part of the debris torus is heated from shocks (to $T \sim 3$ MeV) that emerge when cool, equatorially inflowing material collides with matter being shed from the central object leading to a butterfly-shaped temperature distribution in the r-z-plane (paper I). The cool equatorial inflow ($T < 1$ MeV) allows heavy nuclei to be present with a mass fraction of $\sim 10\%$, these nuclei typically have mass numbers $A \sim 80$ and $Z/A \sim 0.3$. The other parts of the inner disc are essentially dissociated into neutrons and protons. We find neutrino luminosities of $\sim 2 \times 10^{53}$ erg/s which are dominated by electron antineutrinos. The mean energies are $\sim 8, \sim 15, 20 - 25$ MeV for electron neutrinos, electron antineutrinos and the heavy lepton neutrinos, respectively.

3 GAMMA-RAY BURST MECHANISMS

The dominant energy from a NS-NS merger can be extracted after a black hole (BH) has formed, rather than during the precursor stage (Rees 1999). The expected outcome of such an encounter (for most presumed equations of state) would be a rapidly spinning BH, orbited by a neutron-rich high-density torus. The binding energy of the orbiting debris, and the spin energy of the BH represent the two main reservoirs. The first provides up to 42% of the rest mass energy of the torus, while the latter can grant up to 29% (for a maximal spin rate) of the mass of the BH itself. Since the orbital velocities of an inspiralling compact binary close to contact reach a substantial fraction of the speed of light, the resulting BH is guaranteed to be rapidly spinning. This effect is more pronounced for softer equations of state since they yield more compact stars. Being more massive, the BH contains an even larger reservoir of energy than the torus.

The central BH will have a mass of about $2.5 M_{\odot}$, while the rest of the material is either tightly bound in a torus of $M_t \sim 0.15 M_{\odot}$ or almost unbound, launched into highly eccentric orbits. A small fraction of a solar mass escapes the system. The extractable energy could amount to several times $10^{53} (M_t/M_{\odot})$ ergs, thus easily satisfying the total apparent isotropic energies inferred for most GRBs at cosmological distances. The amount of thermal and kinetic energy of both the central object and the debris are given in Table 1. When comparing different runs the reader should keep in mind that they are not all calculated exactly at the same time. They

are divided into contributions from the central object (“> 13”); corresponding to densities above $10^{13} \text{ g cm}^{-3}$) and those from the orbiting debris (“< 13”). Typically (run C), the differentially rotating central object contains $2 \times 10^{52} \text{ erg}$ and $8 \times 10^{52} \text{ erg}$ in thermal and kinetic energy, respectively. In the debris, the kinetic energy dominates by almost an order of magnitude ($\sim 10^{52}$ versus $\sim 10^{51}$ ergs). The corotating runs (A, B, D) yield smaller thermal energy contributions from the central object (very smooth merger process), but substantially more kinetic energy is found in the low density regime (due to the larger initial angular momentum).

How can the available energy now be transformed into outflowing relativistic plasma after such a coalescence event? As argued above, we consider two options, both of which are sketched in Figure 1. A fraction of the energy released as neutrinos is expected to be converted, via collisions, into electron-positron pairs and photons. Neutrinos can give rise to a relativistic, pair-dominated wind if they are converted into pairs in a region of low baryon density (Fig. 1a). Alternatively, strong magnetic fields anchored in the dense matter could convert the gravitational binding energy of the system into a Poynting-dominated outflow (Fig. 1b). A detailed assessment of the viability of both mechanisms follows.

3.1 Neutrino processes

The hot and dense merger remnant is opaque to most forms of radiation. Only neutrinos can extract the large thermal energies stored in the remnant on a short time scale ($\sim 1 \text{ s}$). While they are essentially trapped inside the central object (optical depths $\tau \sim 10^4$), they can leave the hot torus after only a few interactions ($1 < \tau < 10$; see paper II). Most neutrinos are produced in the neutron rich ($Y_e \sim 0.1$) debris torus around the central object, which exhibits temperatures well above the pair production threshold. The conditions in the debris favour positron capture on free neutrons over electron captures and therefore electron anti-neutrinos dominate the neutrino luminosities. For details concerning the neutrino emission we refer to paper II.

The neutrino emission is mildly focused around the rotation axis, an observer looking down on the remnant along the original binary rotation axis would see it around 25 times neutrino brighter than in an edge-on observer. It is in the region above the poles of the merged remnant, surrounded by the high-density walls of the thick disk, where $\nu\bar{\nu}$ annihilation could accelerate a relativistic outflow. Neutrinos emitted from the inner shock-heated regions of the debris, will also deposit part of their energy in the remnant thus driving an energetic baryonic wind (see Fig. 1a). Let us first consider the $\nu\bar{\nu}$ annihilation.

3.1.1 $\nu\bar{\nu}$ annihilation

The annihilation of neutrinos and antineutrinos into e^\pm as a mechanism to power GRBs has been calculated by several groups (Jaroszynski 1993, Mochkovitch et al. 1993, Ruffert et al. 1997b, Popham et al. 1999, Ruffert & Janka 1999, Asano & Fukuyama 2000, 2001, Salmonson & Wilson 2001). To obtain a highly relativistic outflow, the energy from the neutrino annihilation needs to be deposited in a baryon-poor region. The funnel above the central object of the merged remnant is an attractive place for this deposition because not only is it close to the central energy source but contains –due to centrifugal forces– only a small number of baryons. Unfortunately the exact densities in this area are numerically very difficult to resolve. There are actually no SPH-particles along the

rotation axis; the finite density estimate results from contributions of particles located in the high-altitude parts of the debris. Due to this effect, better resolved simulations will yield steeper density gradients towards the z-axis. This is indeed confirmed by comparing the results from run D and B. The density estimates along the z-axis of the merged remnant therefore have to be considered as upper limits. The density contours found in the simulations are shown in the left column of Fig. 2.

We analyse the annihilation of neutrino pairs in a post-processing approach since it is currently not feasible to perform such an expensive calculation together with a full 3D hydro simulation. For the calculation of the neutrino annihilation we follow the approach described in Ruffert et al. (1997), i.e. the following assumptions are made: (i) relativistic effects are ignored since they are not included in the hydrodynamics calculations either; (ii) neutrinos are considered to be emitted isotropically into the half-space determined by the vector $\hat{n} = -\nabla\rho/|\nabla\rho|$; and (iii) the particle distribution in the upper half-space of the remnant is covered with a 3D Cartesian grid (121 x 121 x 41 grid cells) and, to avoid additional complications due to projection effects, a grid cell of volume $(\Delta x)^3$ is replaced by a sphere of the same volume (i.e. $R = (\frac{3}{4\pi})^{1/3} \Delta x$). The discretized form of the energy deposition rate per volume ($\text{erg s}^{-1} \text{ cm}^{-3}$) is then given by

$$\begin{aligned} Q_{\nu\bar{\nu}}(\vec{r}) &= \sum_{i=e,\mu,\tau} Q_{\nu_i\bar{\nu}_i}(\vec{r}) \\ &= \sum_{i=e,\mu,\tau} A_{1,i} \sum_k \frac{L_{\nu_i}^k}{d_k^2} \sum_{k'} \frac{L_{\bar{\nu}_i}^{k'}}{d_{k'}^2} [\langle E_{\nu_i} \rangle^k + \langle E_{\bar{\nu}_i} \rangle^{k'}] \mu_{kk'}^2 \\ &+ \sum_{i=e,\mu,\tau} A_{2,i} \sum_k \frac{L_{\nu_i}^k}{d_k^2} \sum_{k'} \frac{L_{\bar{\nu}_i}^{k'}}{d_{k'}^2} \frac{\langle E_{\nu_i} \rangle^k + \langle E_{\bar{\nu}_i} \rangle^{k'}}{\langle E_{\nu_i} \rangle^k \langle E_{\bar{\nu}_i} \rangle^{k'}} \mu_{kk'} \quad (1) \end{aligned}$$

where the index i labels the type of neutrino. Here L^k is the neutrino luminosity of grid cell k , d_k is the distance from the centre of grid cell k to the point \vec{r} , $d_k = |\vec{r} - \vec{r}_k|$, $\langle E_{\nu_i} \rangle^k$ is the average neutrino energy in grid cell k , $\mu_{kk'} = 1 - \cos \theta_{kk'}$ and $\theta_{kk'}$ is the angle at which neutrinos from cell k encounter anti-neutrinos from cell k' at the point \vec{r} . These relations are sketched in Fig. 3. The constants are given by $A_{1,e} = \frac{1}{12\pi^2} \frac{\sigma_0}{c(m_e c^2)^2} [(C_V - C_A)^2 + (C_V + C_A)^2]$, $A_{1,\mu} = A_{1,\tau} = \frac{1}{12\pi^2} \frac{\sigma_0}{c(m_e c^2)^2} [(C_V - C_A)^2 + (C_V + C_A - 2)^2]$, $A_{2,e} = \frac{1}{6\pi^2} \frac{\sigma_0}{c} [2C_V^2 - C_A^2]$, $A_{2,\mu} = A_{2,\tau} = \frac{1}{6\pi^2} \frac{\sigma_0}{c} [2(C_V - 1)^2 - (C_A - 1)^2]$, where $C_V = 1/2 + 2 \sin^2 \theta_W$, $C_A = 1/2$, $\sin^2 \theta_W = 0.23$ and $\sigma_0 = 1.76 \times 10^{-44} \text{ cm}^2$.

The annihilation calculation is computationally extremely expensive since, in principle, a loop over all *pairs* of grid cells is necessary to get the annihilation rate $Q(\vec{r}, t)$ in a single space-time point, see equation (1). Since it is at present not feasible to calculate the $\nu\bar{\nu}$ annihilation for every time slice, we only perform it at the end of the simulation where the neutrino luminosities have reached their final, stationary levels (apart from maybe run C; see Figs. 2-4 in paper II). We assume mirror symmetry with respect to the orbital plane, i.e. we only calculate $Q(\vec{r})$ in the upper half-plane, which is an excellent approximation for the systems considered here.

In order to further reduce the computational load, we determine in a preprocessing step the number of grid cells that have non-negligible contributions to the annihilation process. Choosing for each neutrino species only those grid cells whose luminosity is above 10^{-2} times the maximum luminosity (of this specific neutrino type), we can reduce the computing time by a factor of $\sim 10^2$ with respect to using all grid cells. The total annihilation

4 Rosswog, Ramirez-Ruiz & Davies

Table 1. Energy reservoirs (in ergs) in the merged remnant. Second column: “cor.”: corotation, “irr.”: no initial spin, “ $\nu+\nu-$ ”: neutrino cooling included/not included, the number refers to the number of SPH-particles used. “kin” refers to kinetic, “therm” to thermal energy. $> / < 13$ indicates whether densities above (“central object”) or below $10^{13} \text{ g cm}^{-3}$ are considered.

run	comments	t_{end} [ms]	$E_{\text{therm}, > 13}$	$E_{\text{kin}, > 13}$	$E_{\text{therm}, < 13}$	$E_{\text{kin}, < 13}$
A	cor., $\nu-$, 207 918	10.7	9.5×10^{51}	4.6×10^{52}	1.8×10^{51}	1.9×10^{52}
B	cor., $\nu-$, 1 005 582	10.8	9.6×10^{51}	4.8×10^{52}	1.9×10^{51}	1.9×10^{52}
C	irr., $\nu+$, 383 470	18.3	2.4×10^{52}	8.0×10^{52}	1.8×10^{51}	1.1×10^{52}
D	cor., $\nu+$, 207 918	20.2	1.3×10^{52}	4.2×10^{52}	3.5×10^{51}	1.9×10^{52}
E	irr., $\nu+$, 750 000	12.2	5.3×10^{52}	1.4×10^{53}	4.7×10^{51}	2.4×10^{52}
F	cor., $\nu+$, 1 005 582	10.7	9.6×10^{51}	4.8×10^{52}	1.9×10^{51}	1.9×10^{52}

rates derived from both methods agree to within 1 %. All these post-processing calculations are performed with a fully parallelised code.

Figure 2 (right column) shows the contours of the (azimuthally averaged) annihilation energy per time and volume, Q . It is in the region along the z -axis where prohibitive baryon loading could be avoided, transforming the $\nu\bar{\nu}$ energy flux into a radiation-dominated fluid with a high entropy per baryon. The thick disc geometry of the remnant with its steep density gradients in the radial direction does not allow for lateral expansion. The only escape route is along the initial binary rotation axis. The disc geometry is therefore responsible for channelling the relativistic outflow into a pair of anti-parallel jets. This mechanism is similar to that envisaged by MacFadyen & Woosley (1999) for the collapsar scenario, but offers the advantage that the jets in our case do not have to pierce through a surrounding stellar mantle.

Figures 4-6 show the ratio of e^\pm energy deposition to baryon rest mass energy, $\eta = Q_{\nu\bar{\nu}}\tau_{\text{inj}}/(\rho c^2)$, in the region above the poles of the merged remnant. η here is calculated by using azimuthally averaged values of both $Q_{\nu\bar{\nu}}$ and ρ (in contrast to those shown in Rosswog & Ramirez-Ruiz 2002 which are in the xz -plane), and can be understood as an indication of the terminal bulk Lorentz factor Γ . The above estimates assume, for simplicity, that the energy deposition rate by $\nu\bar{\nu}$ annihilation into e^\pm pairs at the displayed time is both representative of the subsequent phases and steady for at least one second (this is clearly an upper limit to the total injected energy over the assumed period $\tau_{\text{inj}} \sim 1$ s). Due to the centrifugal evacuation of the funnels the largest Lorentz factors are found along the binary rotation axis and therefore neutrino annihilation will result in a pair of relativistic jets. For our most realistic case, run C, we find peak asymptotic Lorentz-factors of $\Gamma_{as} \approx \eta \approx 15$. This value is certainly resolution biased, with higher resolution resulting in larger Lorentz-factors. For example, for the corotating run D, we find peak Lorentz-factors of $\sim 10^2$, while for the additional, corotating run F (see Table 1), which was not included in papers I and II, we find a peak Lorentz-factor of $\Gamma_{as} \sim 10^5$ see Figure 5. Corotation is certainly a somewhat artificial initial condition (see Bildsten and Cutler 1992), but in the light of this result we do not consider the observational constraints on the Lorentz-factors of GRB-outflows of several hundred (Lithwick and Sari 2001) to be a serious problem. At large angles away from the rotation axis an increasing degree of entrainment leads to a drastic decrease in η (see Figs. 4-6). A broad velocity profile is likely to develop so that different parts move with different Lorentz factors. This is expected to lead to a mixing instability, which may provide the erratic changes of the Lorentz-factor that will cause substantial irregular-

ity or intermittency in the overall outflow that would manifest itself in internal shocks (e.g. Rees & Mészáros 1994; Ramirez-Ruiz & Lloyd-Ronning 2002)

Typical energies of 3×10^{48} erg (run C), 2×10^{47} erg (run D) and 2×10^{49} erg (run E) are found in the jet with $\eta > 1$ (see Fig. 2 in Rosswog and Ramirez-Ruiz 2002). For $\nu\bar{\nu}$ annihilation from neutron star mergers to be the driving mechanism behind short GRBs, substantial beaming, $\Omega_{\nu\bar{\nu}} < 10^{-2}$, is needed to satisfy the requirements on the apparent isotropized energies of $\sim 10^{51}$ erg implied for *short-hard* bursts at $z = 1$ (Panaitescu, Kumar & Narayan 2001; Lazzati et al. 2001). Possible beaming mechanisms are discussed below.

3.1.2 Neutrino-driven winds

A fraction of the neutrino energy emitted from the inner regions of the debris will be deposited in the other parts of the remnant (Fig. 1a), heating and driving material from its surface (Woosley 1993; Ruffert et al. 1997). For example, a nucleon located at ~ 100 km from the central object gains the equivalent of its gravitational binding energy by capturing 3 neutrinos of ~ 15 MeV. Using typical numbers from our simulations, we find that the neutrinos will drive a mass outflow at a rate (Qian & Woosley 1996):

$$\dot{M} \approx 2 \times 10^{-2} M_\odot / \text{s} \quad L_{\bar{\nu}_e, 5.3}^{5/3} \left(\frac{\epsilon_{\bar{\nu}_e}}{15 \text{ MeV}} \right)^{10/3} \left(\frac{R_{\text{em}}}{80 \text{ km}} \right)^{5/3} \left(\frac{2.5 M_\odot}{M_{\text{em}}} \right)^2, \quad (2)$$

where $L_{\bar{\nu}_e}$ is the luminosity in $\bar{\nu}_e$ -neutrinos, $\epsilon_{\bar{\nu}_e} = \frac{\langle E_{\bar{\nu}_e}^2 \rangle}{\langle E_{\bar{\nu}_e} \rangle}$, $E_{\bar{\nu}_e}$ denotes the neutrino energy, R_{em} and M_{em} are the radius of and the mass enclosed in the neutrino emitting region. This estimate is consistent with those found by Woosley (1993) and Duncan, Shapiro & Wassermann (1986). This wind accelerates the blown-off material to its asymptotic velocities of a few 10^9 cm s^{-1} .

3.1.3 Hydrodynamic collimation

As shown above, the question of whether or not $\nu\bar{\nu}$ annihilation is a viable candidate for driving GRBs depends on the possibility of collimating the plasma into a narrow beam. We will briefly summarize a beaming mechanism related to the neutrino-driven wind (beaming by *hoop stresses* produced by the toroidal component of a magnetic field configuration will be addressed later). The wind mechanism is based on the idea of Levinson & Eichler (2000) that the pressure and inertia of a baryonic wind can lead to the collimation of a baryon-poor jet, the detailed assessment of the wind-jet interaction for the neutron star merger case is worked out in Rosswog & Ramirez-Ruiz (2003). The main result is that bursts produced by

such a mechanism are not isotropic but instead beamed within a solid angle, with opening half-angles of

$$\theta \approx \frac{\pi}{\beta_w} \frac{L_j}{L_w} \approx 0.3 \beta_{w,-1}^{-1} L_{w,50}^{-1} L_{j,48.5}, \quad (3)$$

and hence the apparent luminosity is

$$L_\Omega \approx \frac{2}{\pi^2} \frac{\beta_w^2 L_w^2}{L_j} = 2 \times 10^{51} \beta_{w,-1}^2 L_{w,51}^2 L_{j,48}^{-1} \text{ erg s}^{-1}, \quad (4)$$

where β_w is the wind terminal velocity in units of the speed of light, L_w and L_j are the total power in the wind and in the jet, and we adopt the convention $Q = 10^x Q_x$, using cgs units. The proportionality of the opening angle on the jet luminosity yields the paradoxical result that, if all other quantities are the same, a low-luminosity jet will appear brighter than a high-luminosity one. We find for our generic run C $\theta \approx 0.1$ and $L_\Omega \approx 10^{51} \text{ erg s}^{-1}$. With this beaming fraction the BATSE detection rate of short GRBs yields a required event rate that comfortably falls into the range of estimated neutron star merger rates (Rosswog & Ramirez-Ruiz 2003). We find that even a relatively narrow distribution of neutron star masses yields a broad distribution of opening angles and apparent luminosities. These distributions can be found in Rosswog & Ramirez-Ruiz (2003). This model leads to a simple physical interpretation of the isotropic luminosities implied for short GRBs at cosmological distances.

If we use the found energy per solid angle and compare it to that of long bursts (Panaitescu & Kumar 2001) we find that the afterglow of short bursts produced in this way should be typically a factor of 50-100 dimmer than those of long bursts (the afterglow energy is roughly proportional to the energy in the outflow). If short GRBs arise from NS-NS or NS-BH binaries merging in the tenuous outskirts of their host galaxies then our chances for detecting radio and optical afterglows of short GRBs are further diminished since the afterglow brightness in these bands is proportional to the square root of the external density. Assuming that the relativistic shocks in long and short GRBs have similar parameters (i.e. $p=2$, magnetic field is 5 % of equipartition) and using a total isotropic energy of 10^{51} erg and a medium density of $n = 10^{-3} \text{ cm}^{-3}$ we can calculate the 2-10 keV flux (for details see Ramirez-Ruiz, Celotti & Rees 2002). This is shown in Fig. 7 as solid line. The best chance of detecting afterglows of short GRBs is with early X-ray observations with *XMM* and *Chandra* within a few days after the GRB. These conclusions are illustrated in Figure 7, which shows the X-ray emission expected for a short GRB afterglow with lower values of $E \approx 10^{51}/4\pi \text{ erg s}^{-1}$ and $n \approx 10^{-3} \text{ cm}^{-3}$ than those found for long duration ones (*solid line*). Also shown are the *Chandra* upper limits for GRB 020531 (Butler et al. 2002) and GRB 021201 (Hurley et al. 2002), for which the afterglow vanished too soon to permit detection.

The question is why these bursts have been detected in γ -rays but not in X-rays or optical, which would have been expected if the X-ray to γ -ray ratio had been comparable to those in long duration GRBs. One simple reason may be that the afterglows of short GRBs are, on average, dimmer than those of long bursts. This speculation is confirmed by the transient and fading hard X-ray emission obtained by summing up the light curves of all the brightest short bursts seen by *BATSE* (Lazzati et al. 2001). Extrapolation of such a signal to later times shows that the typical short GRB afterglow is close to the current detection limits (*grey region* in Fig. 7). We note that there are short GRBs with fluences significantly larger than average. These bursts could be as energetic as some long GRBs for which afterglows have been seen (and may contribute significantly

to the average signal shown in Fig. 7). The afterglows of such short GRBs could be detected beyond a day with *XMM*.

3.2 Magnetic processes

In this paragraph, we discuss some general ways by which gravity, angular momentum and electromagnetic field could conspire to power GRBs (see e.g. Narayan et al. 1992, Thompson and Duncan 1993, Usov 1992, 1994, Mészáros & Rees 1997, Katz 1997; for a more complete bibliography see the reviews of Piran 1999 and Mészáros 2002). There is considerable literature on the launching of electromagnetically driven jets from the surface of an accretion disc, under the assumption that the disc is threaded by a suitably configured poloidal magnetic field (e.g. Blandford & Payne 1982) but with little discussion of how the field configuration was set up in the first place.

The merger remnant with its large magnetic seed fields and its turbulent fluid motion will give rise to a plethora of electromagnetic activity. We expect coronal arches, as well as larger scale magnetic structures to be quite common and to be regenerated on an orbital timescale. Field lines will be stretched across the disc surface and will quickly be forced to reconnect. Differential rotation will cause loops to twist and probably to undergo some topological rearrangement (Fig. 1b). This provides an alternative mechanism for heating the disc corona and perhaps for driving an outflow through thermal heating (similar to the neutrino heating mechanism described above). Starting with the typical fields of a neutron star the turbulent flow and the differential rotation within the remnant will quickly increase the magnetic field to enormous strengths. The disc may be threaded by a vertical field and differential rotation will make the field approximately axisymmetric. Not only will this create a very effective coupling between the disc and some possible outflow but it can also facilitate the outflow by launching it either centrifugally or through magnetic pressure associated with coiled up toroidal field. There is also a possible magnetic connection between the disc and the hole (e.g. Blandford & Znajek 1997; hereafter B-Z) which can be used to extract the energy stored in the rotation of space-time. But even before the BH forms, a NS-NS merging system might lead to winding up of the fields. This field amplification will continue until the magnetic pressure becomes comparable to the gas pressure at which point the magnetic field becomes buoyant, floats up and forms a magnetically structured corona above the merger remnant.

We will now assess several mechanisms to produce a GRB in more detail.

3.2.1 Energy extraction from the central, supermassive neutron star

In the following we will assume that the central object remains stable against gravitational collapse for the time scale that is of interest for the discussed mechanism. We regard differential rotation to be responsible for this stabilization and expect a large range of possible lifetimes (see discussion in Rosswog & Davies 2002 and Rosswog & Ramirez-Ruiz 2002).

The DROCO mechanism

Kluźniak and Ruderman (1998) have suggested Differentially Rotating Collapsed Objects, so-called DROCOs, as central engines of GRBs. The DROCO will wind up initial seed magnetic fields by differential rotation until the magnetic pressure, $p_{\text{mag}} = B^2/8\pi$

becomes comparable to the matter pressure, i.e. $B \approx B^{\text{eq}}$. At this point the magnetic toroids created by winding up magnetic fields around the rotation axis (the Taylor-Proudman steady state) will become buoyant, float up and finally break through the surface where they will create an ultrarelativistic blast. This mechanism -winding up of the field lines, buoyancy and breaking through the surface- will continue until either the kinetic energy of the DROCO is used up or the central object undergoes gravitational collapse to a black hole. In this way a series of erratic, explosive releases of energy (“sub-bursts”) is created.

The hot, supermassive “neutron star” in the center of merger remnant is rapidly differentially rotating with periods ranging from 0.3 ms to 2 ms (see Figure 10 in Rosswog & Davies 2002) and therefore one such realization of a DROCO. The local saturation field amplitude is determined by a balance between nonlinear growth, dissipative processes like reconnection and buoyant escape and can clearly only be estimated through careful, three dimensional, numerical simulations which are just now becoming possible. Ideally, this process should be treated with general relativistic MHD, but lacking the corresponding tools we will use here a simple toy model together with numbers inferred from our purely hydrodynamic simulations to get a first handle on the possible magnetic properties of the remnant. We will only consider the simplest case of field amplification, the winding up of field lines by differential rotation (a detailed discussion of differential rotation and stellar magnetic fields can be found, for example, in Spruit 1999).

In the left panel of Fig. 8 we plot the equipartition field strengths of the matter distribution of our generic case, run C (at 14.11 ms),

$$B^{\text{eq}} = \sqrt{8\pi\rho c_s^2}, \quad (5)$$

where we have used azimuthally averaged values for the densities and the sound velocity, c_s , which we derived from our nuclear EOS. The equipartition field distribution for the other cases is very similar and is therefore not shown. We find values between 10^{16} and 10^{18} G in the central object ($r_{\text{cyl}} < 30$ km), while the inner parts of the dense torus ($r_{\text{cyl}} < 130$ km) exhibit values between a few times 10^{14} and 10^{16} G. The rapidly expanding low-density regimes ($r_{\text{cyl}} > 130$ km) still yield values well above 10^{13} G. Most of this material moves on eccentric orbits around the centre of mass and will later rain down on the inner parts of the disc thereby refuelling via shock heating the thermal energy reservoir of the torus.

Interactions between the fluid motions \vec{v} and the magnetic fields \vec{B} are governed by the induction equation. If magnetic diffusion is unimportant for the time scales considered here, it reads

$$\partial_t \vec{B} = \nabla \times (\vec{v} \times \vec{B}). \quad (6)$$

If we further assume that the motion of the material can be approximated by an axisymmetric, purely azimuthal motion, the poloidal field component, B_p , does not change in time, but the azimuthal component, B_ϕ is increased by “winding-up” according to

$$B_\phi = 2\pi N(t)B_p, \quad (7)$$

where $N(t)$ is the number of revolutions performed as a function of time. If we assume for simplicity the rotation rate to be stationary on the time scale of interest (in reality magnetic braking will occur), we can write the time it takes B_ϕ to reach equipartition as

$$\tau^{\text{eq}} = \frac{B^{\text{eq}}}{B_p} \omega(r)^{-1}. \quad (8)$$

We evaluate equation (8) for our generic case, run C, at a time where the inner parts of the remnant (central object + high-density part of the disc) have reached a state of stationary rotation (t=

14.11 ms). This is shown in the right panel of Figure 8 as a function of radius where we have used a typical neutron star magnetic field as initial seed, $B_p = 10^{12}$ G. The curve reflects the interplay between the radial dependencies of ω and B^{eq} . Under the above assumptions the central object will reach equipartition within a few 10 s, the high-density torus within ~ 4 s.

Starting from a seed field of 10^{12} G our simple model for the field evolution predicts that it takes around 160 revolutions or 0.3 seconds for the central object to reach a typical magnetar field strength of 10^{15} G. Equipartition, a few times 10^{17} G, will be reached after a few 10 s, the exact time depending on the position within the central object. At this point strongly magnetised flux tubes will float up at roughly the Alfvén speed, $v_A = B/\sqrt{4\pi\rho}$ on a time scale $\tau_b \sim R_{\text{co}}/v_A \approx 1.5 \times 10^{-4}$ s. This short rise time is consistent with observed GRBs that reach their peak luminosity within milliseconds. Kluzniak and Ruderman estimate the energy of a typical sub-burst to be $\sim 10^{51}$ ergs. Using this number and the kinetic energies in the central objects, a few times 10^{52} ergs (Table 1), the central object could launch several tens of such sub-bursts.

Convective motion, dynamos and superpulsars

In the previous section only the relatively slow wrapping of field lines was considered. An effective $\alpha - \omega$ dynamo (Thompson and Duncan 1993) or a magnetorotational instability (Balbus and Hawley 1991, 1998), however, might amplify an initial seed field exponentially on a much shorter time scale.

Figure 9 shows the velocity field in the interior of the central object of run C. It shows “convective cells” of a scale $l_c \sim 1$ km and convective velocities of $v_{\text{con}} \sim 10^8$ cm/s created by fluid instabilities in the course of the merger. Moreover, the neutrino optical depth drops steeply from $\sim 10^4$ in the interior towards the edge of the central object (see Figure 11 in Rosswog and Liebendörfer, 2003). These outer layers lose neutrinos, and therefore lepton number and entropy, at a much higher rate than the interior, thereby creating negative entropy and lepton number gradients (for the neutrino luminosity per volume see Figure 6, second panel, Rosswog and Liebendörfer, 2003), which, in turn, will drive vigorous convection (e.g. Epstein 1979, Burrows and Lattimer 1988). Apart from being roughly twice as massive and more neutron rich ($Y_e \sim 0.1$ rather than ~ 0.3 ; since the individual neutron stars have been deleptonized in the cooling phase after their formation) this state resembles closely the convection phase after the birth of a protoneutron star in a type II supernova. If we assume neutrinos to be the dominant source of viscosity, $\nu_\nu = 10^9 \cdot f(y_p) \cdot T_{15} \cdot \rho_{14}^{-4/3}$ cm²/s (Thompson and Duncan 1993) with $f(y_p) = [y_p^{1/3} + (1 - y_p)^{-1/3}]^{-1}$, $T_{15} = T/15$ MeV, $\rho_{14} = \rho/10^{14}$ gcm⁻³ and y_p the proton fraction, the Reynolds number inside the central object is $Re = v_{\text{con}} l_c / \nu_\nu \sim \text{few } 10^4$. The related viscous damping time scale for the convective motion is $\tau_c \sim l_c^2 / \nu_\nu \sim 60$ s, corresponding to several 10^5 neutron star dynamical time scales.

Whether such a neutron star can support a dynamo is determined by the Rossby number (Duncan and Thompson 1992), $Ro \equiv T_{\text{rot}}/\tau_{\text{con}}$, where T_{rot} and τ_{con} are the rotation period and the convective overturn time, respectively. An effective large scale helical dynamo can only be supported for $Ro < 1$. With our typical convective velocities and cell sizes the convective overturn times are $\tau_{\text{con}} \approx 3$ ms. The rotational periods in the central object are $0.3 < T_{\text{rot}} < 2$ ms (see Figure 10 in Rosswog and Davies 2002), yielding Rossby numbers $0.1 < Ro < 0.7$. We therefore expect a very strong dynamo to be operating. Using the kinetic energy of

the central object of our generic run C, $E_{\text{kin}} = 8 \cdot 10^{52}$ erg (see Table 1), we find that enough energy is available for an average field strength $\langle B \rangle_{\text{co}} = \sqrt{3 \cdot E_{\text{kin}}/R_{\text{co}}^3} \approx 3 \cdot 10^{17}$ G, where R_{co} is the radius of the central object. This is in good agreement with the equipartition field strengths shown in Figure 8.

Such a convective dynamo amplifies seed magnetic fields exponentially with an e-folding time, τ close to the convective time scale (Nordlund et al. 1992). Using the numbers from our simulation equipartition will be reached in the central object after only $\tau^{eq} = \tau \ln(B^{eq}/B_0) \approx 38$ ms.

Such an object could act like the “superpulsar” envisaged by Usov (1992). The kinetic energy from the deceleration of the central object is released in the form of an (initially) optically thick electron positron wind with frozen-in magnetic field. Once the magnetohydrodynamic approximation breaks down far from the pulsar, electromagnetic waves are generated that accelerate outflowing particles to ultrarelativistic Lorentz factors (10^6 or more; Usov 1994). Using typical numbers from the simulation and $B = \langle B \rangle_{\text{co}} = 3 \cdot 10^{17}$ G as estimated above the magnetic dipole luminosity is

$$L_{\text{md}} = 5.1 \cdot 10^{53} \text{ erg/s} \left(\frac{B}{3 \cdot 10^{17} \text{ G}} \right)^2 \left(\frac{R}{15 \text{ km}} \right)^6 \left(\frac{\omega}{3000 \text{ 1/s}} \right)^4 \quad (9)$$

and the spin down time scale will be $\tau_{\text{sd}} = E_{\text{kin}}/L_{\text{md}} \approx 0.2$ s, which maybe not just by chance coincides with the typical duration of a short GRB.

3.2.2 Energy extraction from a central black hole: the Blandford-Znajek mechanism

Although the time scale is uncertain, the central part of the merger remnant will sooner or later collapse to a rotating BH (unless nuclear physics allows the support of cold objects of $2.8 M_{\odot}$). If magnetic fields of comparable strength to those discussed above thread the BH, its rotational energy of

$$E_{\text{rot}} = M_{\text{bh}} c^2 \left(1 - \sqrt{1/2 \left(1 + \sqrt{1 - a^2} \right)} \right) \approx 1.5 \times 10^{53} \text{ erg}, \quad (10)$$

can be extracted via the B-Z process (Blandford and Znajek 1977). Here $a = Jc/GM^2$ is the BH rotation parameter. The above estimate has been calculated using typical numbers from our simulations ($M_{\text{bh}} = 2.5 M_{\odot}$ and $a = 0.5$). The relevant field component for the energy extraction via the BZ-process is the poloidal field. The ratio between the poloidal and azimuthal field is given by $B_p/B_{\phi} \approx (H/R)$ (Meier 2001). For the thick disks under consideration $H \sim R$ (see Fig. 2, left panels) and therefore we use $B = B_p \approx B_{\phi}$. If the BH is threaded by the equipartition magnetic field of the disc $\approx 3 \times 10^{15}$ G then a jet with luminosity $L_{\text{jet}} = B^2 H^2 R^2 \Omega^2 / 32c \approx 10^{53} \text{ erg s}^{-1}$ (Meier 2001) will result. Again, the typical time scale will be of the order of a typical short GRB duration: $\tau_{\text{BH}} = E_{\text{rot}}/L_{\text{jet}} \approx 1.5$ s.

3.2.3 Energy extraction from the disk

Very similar processes are expected to take place in the disc (Narayan et al. 1992). After around 4 s the field strength has reached equipartition, $\sim 10^{15}$ G, and the field will float up to the disk surface in $\tau_b \sim H/v_A \approx 2 \times 10^{-2}$ s where it will form a magnetically structured disk corona. Livio et al. (1999) estimate a maximum possible disc luminosity (Poynting flux or magnetically driven wind) given by

$$L_{\text{disk}}^{\text{max}} \sim \frac{B^2}{4} R^3 \omega \approx 5 \times 10^{52} \text{ erg s}^{-1}, \quad (11)$$

where we have used the numerical values found at the outer edge of the thick debris disk (see Fig. 8) and assumed that both the poloidal and azimuthal fields are of comparable strength. Even allowing for only 10 % of this luminosity to be converted into an MHD jet, a system powered by the disc binding energy would –without beaming– satisfy the apparent isotropized energy of 10^{51} ergs implied for short-hard bursts at $z \approx 1$ (Panaitescu et al. 2001; Lazzati et al. 2001). The disk would allow an energy extraction on a possibly longer time scale than the central object, $\tau_{\text{disk}} = E_{\text{disk}}/L_{\text{disk}}^{\text{max}} > 0.42 \cdot M_{\text{disk}} c^2 / L_{\text{disk}}^{\text{max}} \sim 3$ s.

4 DISTRIBUTION OF NEUTRON STAR MERGERS WITH RESPECT TO THEIR HOST GALAXIES

The distribution of neutron–star mergers with respect to their host galaxies depends on the distribution of the times it takes from the formation of the system to coalescence and, of course, on the galactic potential. All formation channels seem likely to produce binaries receiving kicks of order 100 – 200 km/s. If the median merger time is approximately 10^6 yr, then a large fraction of mergers will occur close to star–formation sites (i.e. within the host galaxy). If, however, the median merger time is closer to 10^8 yr, then a large fraction of mergers may occur somewhat outside their host galaxies (which are typically dwarf galaxies). Searches for host galaxies of gamma–ray bursts may thus help limit the possible progenitors (see e.g. Bloom et al. 2002) *providing* we have a reasonable understanding of the distribution of merger times and accurate galactic models.

The merger time due to gravitational radiation is a sensitive function of separation a , $\tau_{\text{gr}} \propto a^4$, and thus slight changes in the initial distribution of separations will lead to much larger variations in the distribution of merger times. There are a number of recent papers concerning the evolutionary pathways to producing NS–NS binaries. Bloom et al. (1999) use the binary evolutionary code of Pols and Marinus (1994) and produce a population with the merger time peaking at about 10^8 yr. Fryer et al. (1999) consider three distinct routes to producing NS–NS binaries and find $\tau_{\text{gr}} \sim 10^8 - 10^9$ yr. More recently, Belczynski et al. (2002a, b, c) argue that a large fraction of mergers should occur on much shorter time scales ($\tau_{\text{gr}} \sim 10^5 - 10^6$ yr). The penultimate stage in producing a NS–NS binary consists of one neutron star in a tight binary with a helium star. The latter will produce the second neutron star when it explodes as a type II supernova. However, if the helium star expands to fill its Roche lobe, the subsequent mass transfer may alter the separation of the two stars and thus affect the distribution of initial separations (and therefore merger times) for the NS–NS binaries. Belczynski et al. argue that this mass transfer produces a common envelope phase, where the neutron star and the core of the helium star spiral together whilst ejecting the helium–star envelope. For typical parameters this process will produce NS–NS binaries having initial separations ~ 0.2 to $\sim 2 R_{\odot}$. Such a population is shown in Figure 10 for $\alpha_{\text{ce}} \lambda_{\text{ce}} = 1$, where α_{ce} is the common envelope efficiency, λ_{ce} is a function of the internal structure of the star and defined as in equation (9) of Davies et al. (2002). We argue, however, that there is a problem with this scenario as a common envelope evolution would require very large common envelope efficiencies to reproduce observed systems. In Figure 10 we

have also plotted the WD-NS binary J1141-6545. This binary was produced in a manner similar to NS-NS binaries (Davies, Ritter & King 2002). According to the scenario suggested in Davies et al. (2002), mass transfer occurs when the helium star fills its Roche lobe but rather than forming a common envelope, the material is ejected by the white dwarf, in a manner similar to the evolution assumed for the X-ray binary Cygnus X-2 (Kolb et al. 2000). If instead we assume mass transfer does produce a common envelope phase, J1141-6545 can only be produced if we assume an extremely high common envelope efficiency, $\alpha_{ce}\lambda_{ce} = 10$, as shown in Fig. 11. But with this high value of α_{ce} the scenario of Belczynski et al. also produces initial separations close to the results found by other workers, leading to median merger times of $\sim 10^8$ yr. In fact, Ivanova et al. (2002) suggest an alternative treatment for the mass transfer, and also produce merger times of $\sim 10^8$ yr.

The distribution of merger times is shown in Figure 12 (solid lines from left to right): the merger timescales envisioned in Belczynski et al. (2002a, b, c), those derived through J1141-6545-like evolution, those derived neglecting the radius of the helium star, and those derived for 2303-like evolution, where the helium star fails to fill its Roche lobe and instead mass-loss occurs via a wind. The dotted line is for the evolution as described in Belczynski et al. (2002a, b) but with $\alpha_{ce}\lambda_{ce} = 10$ which is required under this scenario to produce the observed system J1141-6545. Figure 12 shows the importance of considering the helium star radius. Those systems filling their Roche lobes produce very tight binaries which have short merger times. But the observed properties of J1141-6545 impose a very important constraint on any evolutionary scenario. With this constraint, all models produce median merger times of about 10^8 yrs.

We want to point out here that the agreement of theoretical distributions of merger sites with observations is a very sensitive function of the assumed galactic potential. Assuming a J1141-6545-like evolution, we performed a monte carlo simulation of the population of neutron star binaries, integrating their motion within a galactic potential and observing their projected distances from the galactic centre when they merge. This is shown in Fig. 13 for three galactic models: models d, b, and e. Models d and b have galactic disc lengthscales of 1 kpc, whereas model e has a galactic disc lengthscale of 3 kpc. The halo scalelengths are 3kpc for all three models. Model b has a total mass of $0.278 \times 10^{11} M_{\odot}$ whereas models d and e have a total mass of $0.625 \times 10^{11} M_{\odot}$ (see Bloom et al. 1999 for further details). We also plot the *observed* distribution from Bloom et al. (2002). The probability that the observed distribution matches the theoretical curves is a sensitive function of galactic potential (model d: 9 %, model b: 4 %, model e: 0.1 %), i.e. just changing the mass of a galaxy by a factor of 2 has a drastic effect on the resulting probabilities. It should be recalled that the observed distribution is for a sample of long GRBs. If the merger of two compact objects produce short bursts, the lack of agreement between the theoretical curves of mergers and observations of long bursts is not a surprise.

5 SUMMARY AND DISCUSSION

We have addressed the viability of binary neutron star coalescences as central engines of GRBs. Two possible forms of outflow have been considered: (i) a pair dominated fireball generated by $\nu\bar{\nu}$ annihilation, and (ii) electromagnetic Poynting flux.

We find that the plasma produced by the annihilation of $\nu\bar{\nu}$ pairs will be channeled by the high-density walls of the thick

disk of the remnant into relativistic, bipolar jets along the original binary rotation axis. In extreme cases we find peak asymptotic Lorentz-factors of up to $\sim 10^5$. The energy contained in these jets, however, falls short of reproducing the isotropized energy requirements, $E_{iso} \sim 10^{51}$ ergs for short bursts at $z \approx 1$ that are deduced from observations. Since we find typical energies of $\sim 10^{48}$ ergs only, $\nu\bar{\nu}$ the emission has to be beamed into a small fraction of the sky in order for $\nu\bar{\nu}$ annihilation to be a viable GRB mechanism. By applying models developed in the context of protoneutron stars produced in core-collapse supernovae we find that the huge neutrino emission of the merger remnant ($\sim 2 \times 10^{53}$ erg/s) will drive a strong baryonic wind with mechanical luminosities of $\sim 10^{50}$ erg s $^{-1}$. This outflow will have enough pressure to provide adequate collimation, satisfying both the isotropized energy requirements and the estimated rate of binary mergers (Rosswog & Ramirez-Ruiz 2003). A second feature of the jet-wind interaction is that there will be some entrainment of the electron-ion plasma and this should show up in the polarization observations, which can, in principle, distinguish a pair plasma from a protonic plasma. Due to entrainment, the jet will develop a velocity profile with velocities decreasing away from the jet axis. This implies that an observer is likely to infer a value of the Lorentz factor that depends upon the inclination of the line of sight to the jet axis. Seen from one viewing angle a burst would appear as a X-ray rich burst (Heise et al. 2001) while from a different angle it would be interpreted as a standard GRB (Salmonson 2000; Ioka & Nakamura 2001; Kobayashi, Ryde & MacFadyen 2002; Ramirez-Ruiz & Lloyd-Ronning 2002; Mészáros et al. 2002). In some cases mixing instabilities at the jet walls could spoil the jet with baryons and result in a non-relativistic, “dirty fireball” rather than a proper GRB fireball. We predict the afterglow of such a burst to be dimmer than those of long bursts by a factor of $\sim 50 - 100$. The best chances to detect such an afterglow are with *XMM* and *Chandra* within a few days after the GRB.

An alternative way to tap the torus energy is via magnetic fields. The large seed magnetic fields of the individual neutron stars will collude with the complex fluid motion in the merger remnant to produce enormous field strengths. This may proceed via pure differential rotation, dynamo action and/or magnetorotational instabilities.

If the central object resulting from the merger does not collapse immediately, it will be subject to vigorous convection. This convection is driven by large entropy and lepton number gradients established via neutrino emission and will resemble the convection in a newborn protoneutron star. We find Rossby numbers well below unity and therefore expect the central object to act as an efficient large scale dynamo amplifying initial seed fields exponentially. We find that enough energy is available to build up field strengths of several times 10^{17} G. The spindown timescale of a “neutron star” endowed with such a field is ~ 0.2 s which coincides with the average duration of a short GRB.

We have investigated several magnetic mechanisms to produce a GRB, considering the extraction of available energy from the supermassive neutron star in the center of the merger remnant, from a black hole that is expected to form at some stage after the merger and from the debris disk. Most of these (apart from perhaps the DROCO mechanism) seem to be able to extract the available energies at rates in excess of 10^{52} ergs/s. Consuming the available energy reservoirs at such rates naturally leads to durations of order one second. These mechanisms are able to satisfy the requirements on the equivalent isotropized energies of short GRBs even without

beaming.

Moreover, such magnetic mechanisms are supported by the recent observation of linear polarization in the prompt gamma-ray emission from GRB021206 (Coburn and Boggs, 2003) which suggests that the GRB explosion is powered by a central engine with a strong, large-scale magnetic field.

Given the plethora of different mechanisms to transform the large gravitational binding energy into gamma-rays, the enormous observed diversity of GRBs seems to be a natural consequence. Several of the discussed mechanisms may be active at the same time. For example, the directed, relativistic jets produced via neutrino annihilation may be accompanied by uncollimated gamma-rays produced in energetic disk flares.

Finally we want to add a word of caution concerning the comparison of theoretical merger site distributions with observed ones. We have reexamined the distribution of merger sites with respect to their host galaxies since this distribution is generally regarded as an important clue the nature of the GRB progenitors. Our Monte Carlo simulations yield median merger times of $\sim 10^8$ years rather than the much shorter times claimed recently and are thus in agreement with several previous results. Using our distribution of merger times we have calculated the projected distances of the merger sites to the galactic centre. We found median distances of ~ 3 kpc, but stress explicitly that the probability that theoretical distributions match observations is very sensitive to the properties assumed for the host galaxy.

ACKNOWLEDGEMENTS

It is a pleasure to thank M. J. Rees and G. Wynn for stimulating discussions and the Leicester supercomputer team S. Poulton, C. Rudge and R. West for their excellent support. The computations reported here were performed using both the UK Astrophysical Fluids Facility (UKAFF) and the University of Leicester Mathematical Modelling Centre's supercomputer. S.R. gratefully acknowledges a PPARC Advanced Fellowship, E.R. was supported by CONAcYT, SEP and the ORS foundation. M.B.D. gratefully acknowledges support of a URF from the Royal Society. Theoretical astrophysics at Leicester is supported by a PPARC rolling grant.

REFERENCES

- Asano K., Fukuyama T., 2000, *ApJ*, 531, 949
 Asano K., Fukuyama T., 2001, *ApJ*, 546, 1019
 Balbus, S.A. & Hawley, J.F., 1991, *ApJ*, 376, 214
 Balbus, S.A. & Hawley, J.F., 1998, *Rev. Mod. Phys.*, 70, 1
 Belczynski, K., Bulik, T. & Kalogera, V., 2002, *ApJ* 571, L147
 Benz W., 1990, in Buchler J., ed., *Numerical Modeling of Stellar Pulsations*. Kluwer Academic Publishers, Dordrecht, p. 269
 Benz W., Bowers R., Cameron A., Press W., 1990, *ApJ*, 348, 647
 Bildsten, L. and Cutler, C., 1992, *ApJ*, 400, 175
 Blandford R.D., Znajek, R.L., 1977, *MNRAS*, 179, 433
 Blandford R.D., Payne D. G., 1982, *MNRAS*, 199, 883
 Blandford R. D., 2002, "Lighthouses of the Universe", *Proc. Symposium held in Garching, Germany (Aug 6-9 2001)* eds. M. Gilfanov, R. Sunyaev et al. Berlin: Springer.
 Bloom J.S., Kulkarni S.R., Djorgovski S.G., 2002, *Astronomical Journal*, 123, 1111
 Butler, N. R., Dullighan, A., Ford, P., Monnelly, G., Ricker, G., Vanderspek, R., Hurley, K., Lamb, D., 2002, *GRB Circular Network*, 1415, 1
 Cavallo, G. & Rees, M.J., *MNRAS*, 1978, 183, 359
 Chevalier R. A., Li Z.-Y., 1999, *ApJ*, 520, L29
 Coburn, W. & Boggs, S.E., 2003, *Nature*, 423, 415
 Davies, M. B., Benz, W., Piran, T. & Thielemann, F. K., 1994, *ApJ*, 431, 742
 Davies, M. B., Ritter, H., King, A.R., 2002, *MNRAS*, 335, 369
 Di Matteo, T., 1998, *MNRAS*, 299, L15
 Duncan, R.C. Shapiro, S.L. & Wasserman, I., 1986, *ApJ*, 309, 141
 Duncan, R.C. & Thompson, C., 1992, *ApJ*, 392, L9
 Eichler D., Livio M., Piran T. & Schramm D.N., 1989, *Nature* 340, 126
 Fryer, C., Woosley, S.E. & Hartmann, D., 1999, *ApJ*, 526, 152
 Hurley, K. et al. 2002, *GCN*, 1741
 Katz, J.I., 1997, *ApJ*, 490, 772
 Kluzniak, W. & Ruderman, M., 1998, *ApJ*, 505, L113
 Lazzati, D., Ramirez-Ruiz, E. & Ghisellini, G., 2001, *A&A*, 379, L39
 Lee, W.H. & Kluzniak, W., 1999, *MNRAS*, 308, 780
 Lee, W.H. & Kluzniak, W., 1999, *ApJ*, 526, 178
 Lee, W.H., 2001, *MNRAS*, 328, 583
 Lee, W.H., 2000, *MNRAS*, 318, 606
 Lee W. H., Ramirez-Ruiz E., 2002, *ApJ*, 577, 893
 Levinson, A. & Eichler, D., 2000, *Phys. Rev. Lett.*, 85, 236
 Lithwick, Y. and Sari, R., 2001, *ApJ*, 555, 540
 MacFadyen, A. I. & Woosley, S. E., 1999, *ApJ*, 524, 262
 MacDonald, D.A., Thorne, K.S., Price, R.H., & Zhang, X.-H., 1986, in *Black Holes: The Membrane Paradigm*, ed. K.S. Thorne, R. Price & D. MacDonald, Yale University Press, New Haven., p. 21
 Meier, D.L., 2001, *ApJ* 548, L9
 Mészáros, P. & Rees, M. J., 1994, *MNRAS*, 269, L41
 Mészáros, P. & Rees, M. J., 1997, *ApJ*, 482, L29
 Mészáros P., Ramirez-Ruiz E., Rees M. J., Zhang B., 2002, *ApJ*, 578, 812
 Mészáros, P., 2002, *Annu. Rev. Astron. Astrophys.*, 40, 137
 Mochkovitch R., Hernanz M., Isern J., Martin, X., 1993, *Nature*, 361, 236
 Monaghan J.J., 1992, *Ann. Rev. Astron. Astrophys.*, 30, 543
 Narayan R., Paczyński B., Piran T., 1992, *ApJ*, 395, L83
 Narayan R., Yi I., 1995, *ApJ*, 444, 231
 Narayan R., Piran T., Kumar P., 2001, *ApJ*, 557, 949
 Nordlund, A., Brandenburg, A., Jennings, R.L., Rieutord, M., Ruokolainen, J., Stein, R.F. and Tuominen, I., 1992, *ApJ*, 392, 647
 Paczyński B., 1986, *ApJ*, 308, L43
 Panaitescu, A., Kumar, P. & Narayan, R., 2001, *ApJ*, 561, L171
 Popham R., Woosley S. E., Fryer C., 1999, *ApJ*, 518, 356
 Piran T., *Physics Reports*, 1999, 314, 575
 Qian, Y.-Z. & Woosley, S. E., 1996, *ApJ*, 471, 331
 Ramirez-Ruiz E., Dray L., Madau P., Tout C. A., 2001, *MNRAS*, 327, 829
 Ramirez-Ruiz E., Lloyd-Ronning N. M., 2002, *NewA*, 7, 197
 Rees M. J., Mészáros P., 1994, *ApJ*, 430, L93
 Rees, M.J., 1999, *A&AS*, 138, 491
 Rosswog, S., Liebendörfer, M., Thielemann, F.-K., Davies, M. B., Benz, W. & Piran, T., 1999, *A&A*, 341, 499
 Rosswog S., Davies M. B., Thielemann F.-K., Piran T., 2000, *A & A*, 360, 171
 Rosswog S., Davies M. B., 2002, *MNRAS*, 334, 481
 Rosswog S., Ramirez-Ruiz E., 2002, *MNRAS*, 336, L7
 Rosswog, S. & Liebendörfer, 2003, *MNRAS*, 342, 673
 Rosswog, S. & Ramirez-Ruiz E., 2003, *MNRAS* in press
 Ruffert M., Janka H.-T., Schäfer G., 1996, *A & A*, 311, 532
 Ruffert M., Janka H.-T., Takahashi K., Schäfer G., 1997, *A & A*, 319, 122
 Ruffert M., Janka H.-T., 1999, *A & A*, 344, 573
 Ruffert M., Janka H.-T., 2001, *A & A*, 380, 544
 Salmonson J. D., 2000, *ApJ*, 544, L115
 Salmonson J. D., Wilson, J. R., 2001, *ApJ* 561, 950
 Shemi, A. & Piran, T., 1990, *ApJL*, 365, 55
 Shen H., Toki H., Oyamatsu K., Sumiyoshi K., 1998a, *Nuclear Physics, A* 637, 435
 Shen H., Toki H., Oyamatsu K., Sumiyoshi K., 1998b, *Prog. Theor. Phys.*, 100, 1013
 Spruit, H.C., 1999, *A&A*, 349, 189
 Stanek, K.Z. et al., 2003, *astro-ph/0304173*
 Thompson, C. & Duncan, R.C., 1993, *ApJ*, 408, 194

Thompson, C., 1994, MNRAS, 270, 480

Usov, V.V., 1992, Nature, 357, 472

Usov, V.V., 1994, MNRAS, 267, 1035

Woosley, S. E., 1993, A&AS, 97, 205

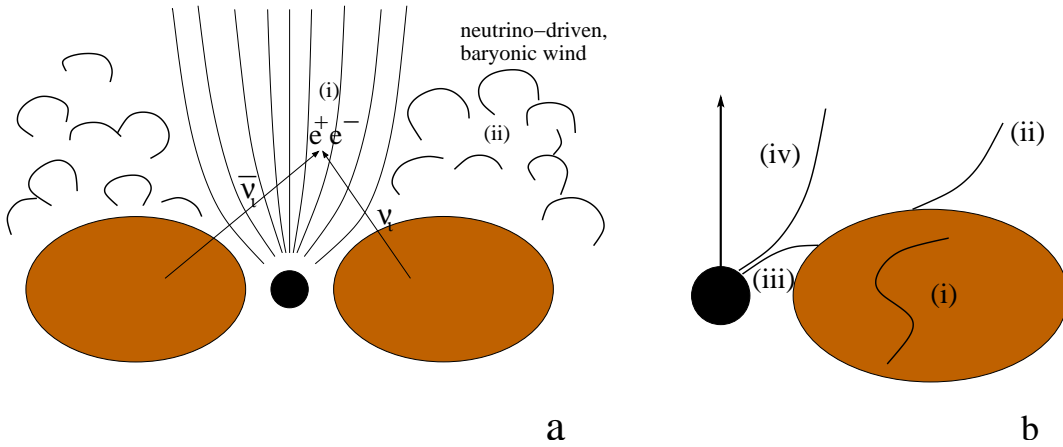


Figure 1. Mechanisms to produce a GRB from a neutron star merger. **Panel a:** neutrinos from the hot remnant annihilate and produce a relativistic outflow (“fireball”, (i)). Moreover, the huge neutrino flux drives an energetic baryonic wind (ii) that collimates the jet. **Panel b:** Strong magnetic fields anchored in the dense matter can convert the binding and/or spin energy into a Poynting outflow. Dynamo processes are believed to operate in accretion discs and physical considerations suggest that fields generated in this way would have a typical length-scale of the order of the disc thickness (i). Open field lines that connect the disk to the outflow can drive a hydromagnetic wind (ii). The above mechanism can tap the binding energy of the debris torus. At some stage after the merger a rapidly spinning black hole is expected to form. Its energy could be extracted in principle through MHD coupling to the rotation of the hole (iii and iv). Panel adapted from Blandford (2002).

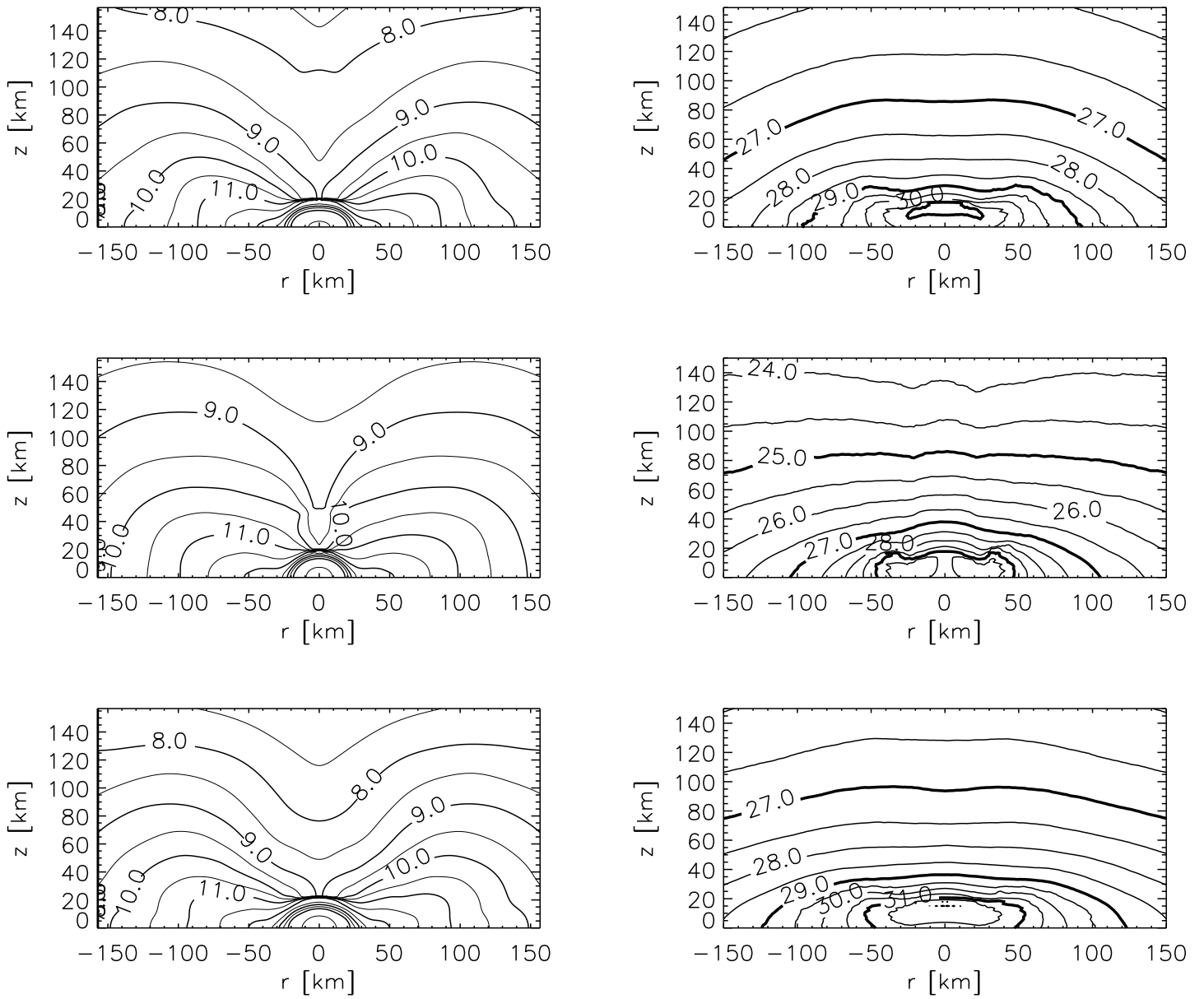


Figure 2. Left panel: densities along the rotation axis of run C, D and E (top to bottom). Right panel: contours of the energy deposited per time and volume (ergs/s cm^3) via $\nu\bar{\nu} \rightarrow e^+e^-$.

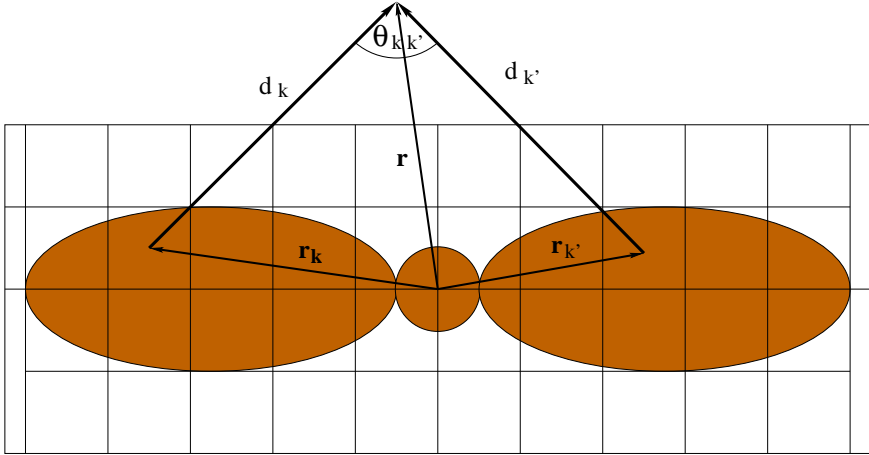


Figure 3. Quantities from eq. (1): sketched is the grid with the vectors needed to evaluate the annihilation at point \vec{r} resulting from neutrinos coming from cell k and anti-neutrinos from cell k' .

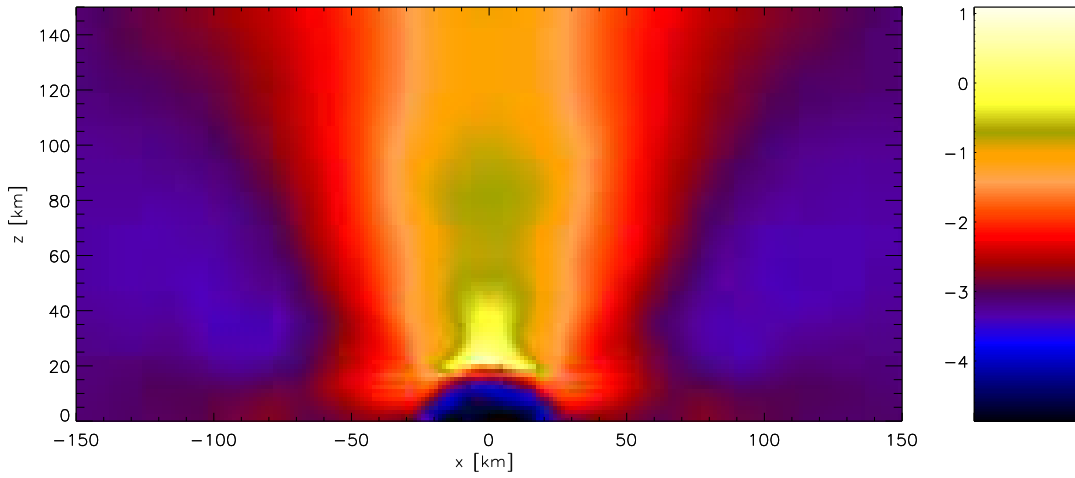


Figure 4. Colour-coded is the ratio of energy deposited via $\nu\bar{\nu} \rightarrow e^+e^-$ to rest mass energy, η , which is a measure of the maximum attainable Lorentz factor. Shown are the values of $\log(\eta)$ in the x - z -plane above the merged remnant of model C (no initial spins, $2 \times 1.4 M_\odot$) at the end of the simulation ($t=18.3$ ms). Due to the symmetry of the merger remnant with respect to the orbital plane a similar jet will occur along the negative z -axis.

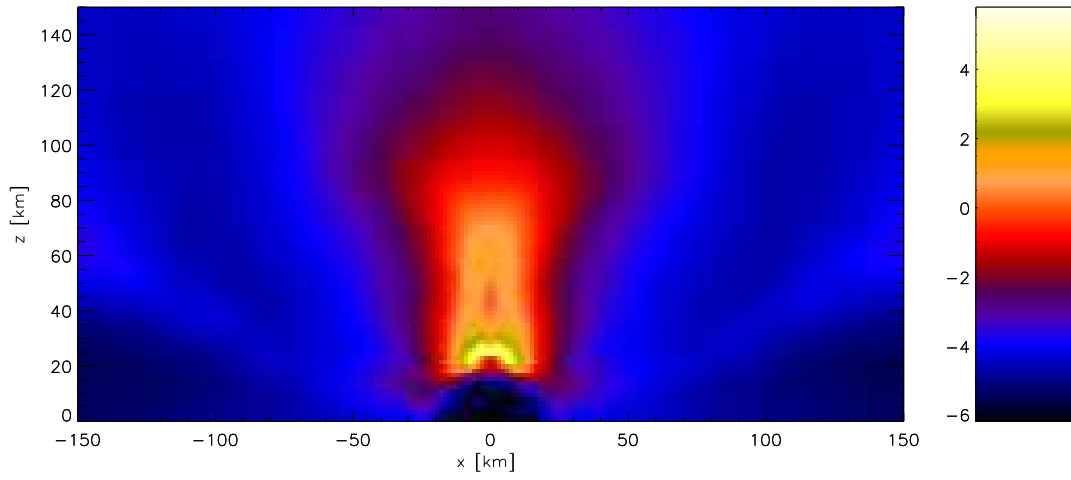


Figure 5. Same as Figure 4, but for an initially corotating binary system, run F (see Table 1).

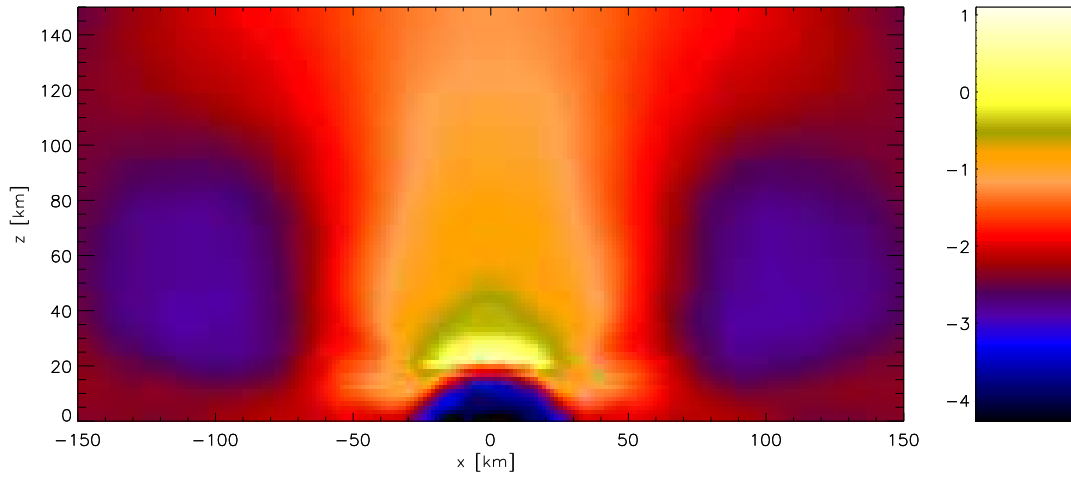


Figure 6. Same as Figure 4, but for our extreme case ($2 \times 2.0 M_{\odot}$, no initial spins)

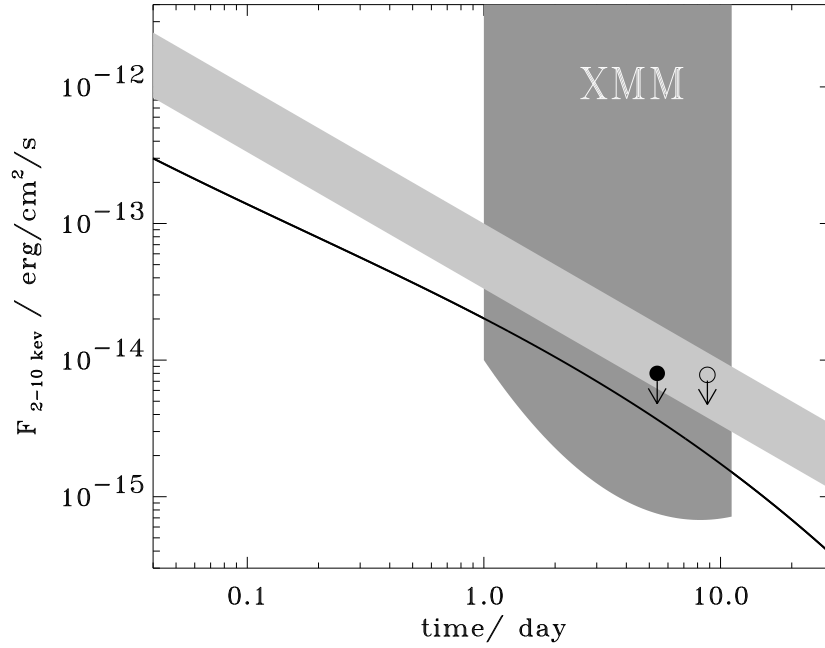


Figure 7. Detectability of short GRBs produced via beamed $\nu\bar{\nu}$ annihilation (see text for details) with *XMM*. The solid line shows the 2-10 keV emission expected from afterglows of short GRBs. Model parameters have been chosen assuming that the relativistic shocks in short and long GRB afterglows have similar parameters except that the average kinetic energy per unit solid angle for short ones is $10^{51}/4\pi$ and the ejecta are collimated, with an initial aperture (half-angle) of 0.1 radians. A low density medium $n \sim 10^{-3}\text{cm}^{-3}$ as expected in NS-NS merger models, has been chosen. The shaded region shows the extrapolated average afterglow emission at X-ray frequencies and later times, assuming a ν^{-1} spectrum (best fit to the measurement of Lazzati et al. 2001) and a t^{-1} decay law. The black dot corresponds to GRB 020531, the open circle to GRB 011201.

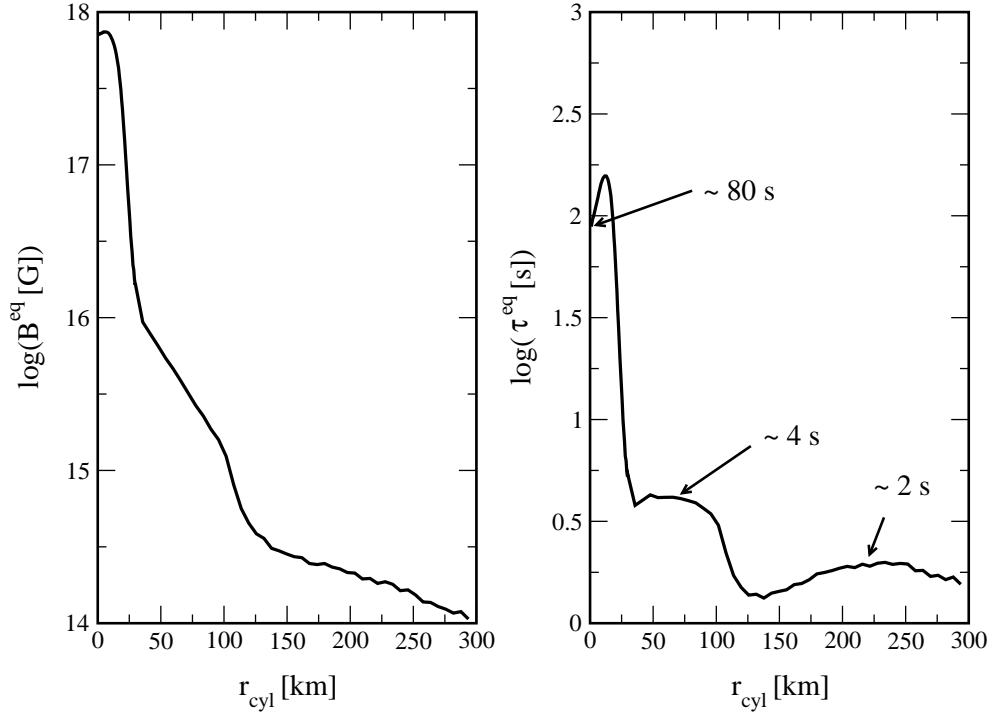


Figure 8. The left panel shows the equipartition magnetic field determined for our generic case, run C at 14.11 ms, from $B^{\text{eq}} = \sqrt{8\pi\rho c_s^2}$. The right panel shows the time it takes to reach the equipartition field strengths, starting with an initial field of $B_0 = 10^{12}$ G. See text for details.

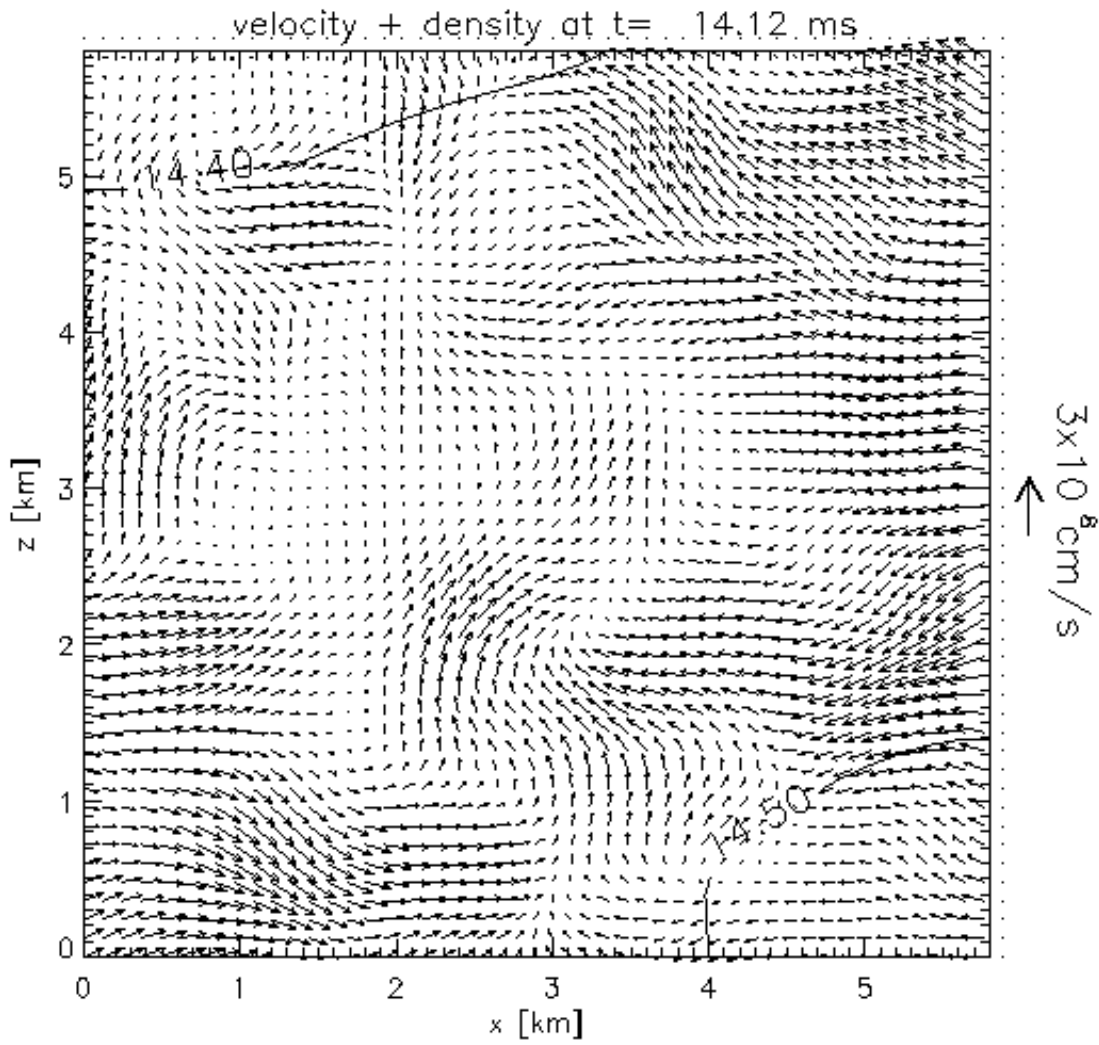


Figure 9. Velocity field inside the central, supermassive neutron star of our generic case ($2 \times 1.4 M_{\odot}$, no initial spin; run C).

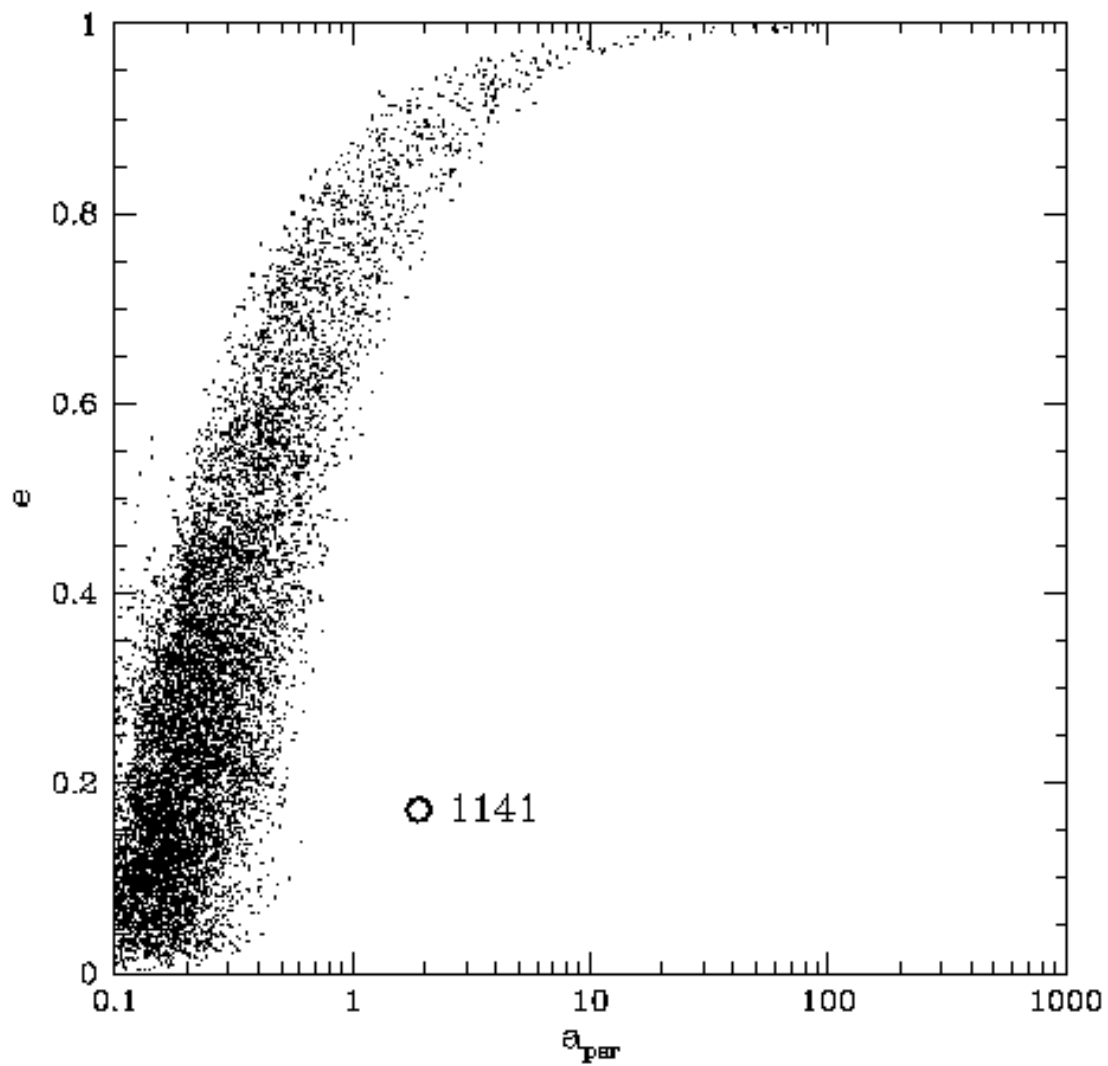


Figure 10. Plot of eccentricity e as a function of separation (in solar radii) for NS–NS systems undergoing a final common envelope phase when the helium star fills its Roche lobe as described in the text. In this plot, $\alpha_{\text{ce}}\lambda_{\text{ce}} = 1.0$ has been used. The open circle is the observed (WD–NS) system J1141–6545.

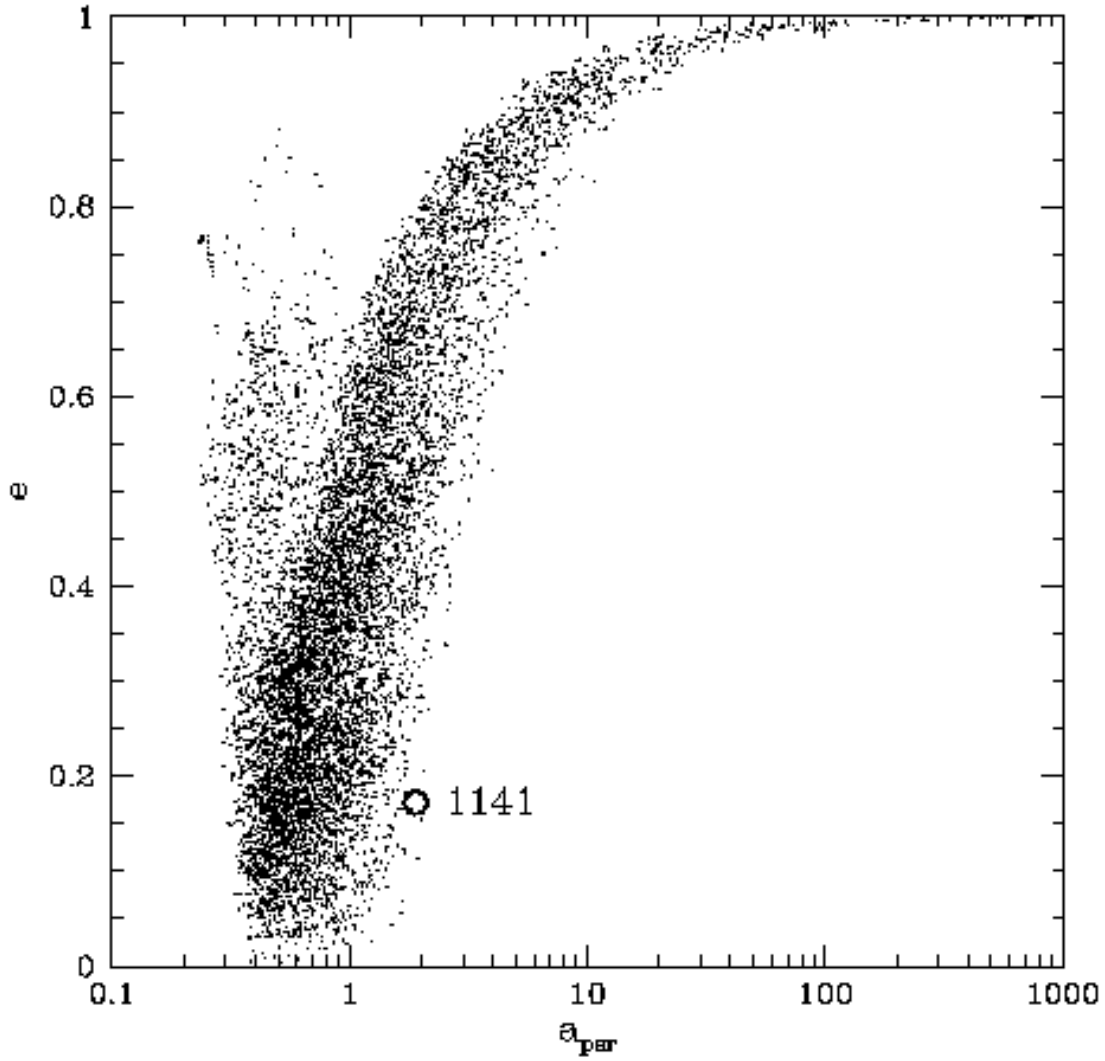


Figure 11. Plot of eccentricity e as a function of separation (in solar radii) for NS–NS systems undergoing a final common envelope phase when the helium star fills its Roche lobe as described in the text. In this plot, $\alpha_{\text{ce}}\lambda_{\text{ce}} = 10.0$. The open circle is the observed (WD–NS) system J1141–6545.

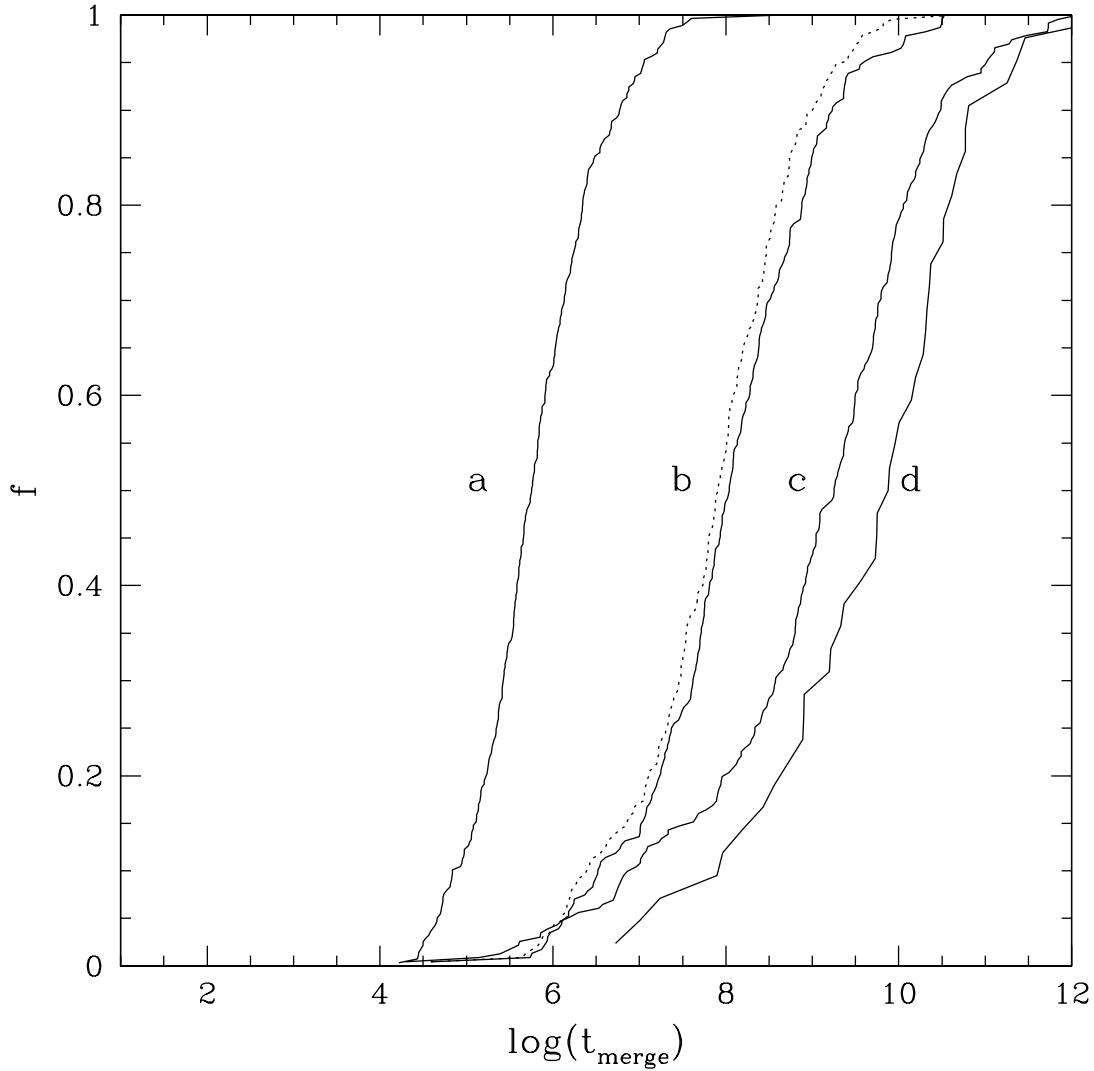


Figure 12. A plot of the cumulative distribution of merger times for neutron star binaries under various assumptions for the formation route. Considering first the four solid lines, from left to right: common envelope phase ($\alpha_{ce}\lambda_{ce} = 1.0$) when helium star fills its Roche lobe (line a); 1141-like evolution (i.e. Cyg X-2 mode of mass transfer occurs when helium star fills its Roche lobe; line b); the distribution obtained when the size of the helium star is neglected (line c); and the distribution obtained for the systems following a 2303-like evolution (ie the helium star fails to fill its Roche lobe and instead mass-loss occurs via a wind; line d). The dotted line is produced assuming a common envelope phase but with $\alpha_{ce}\lambda_{ce} = 10.0$.

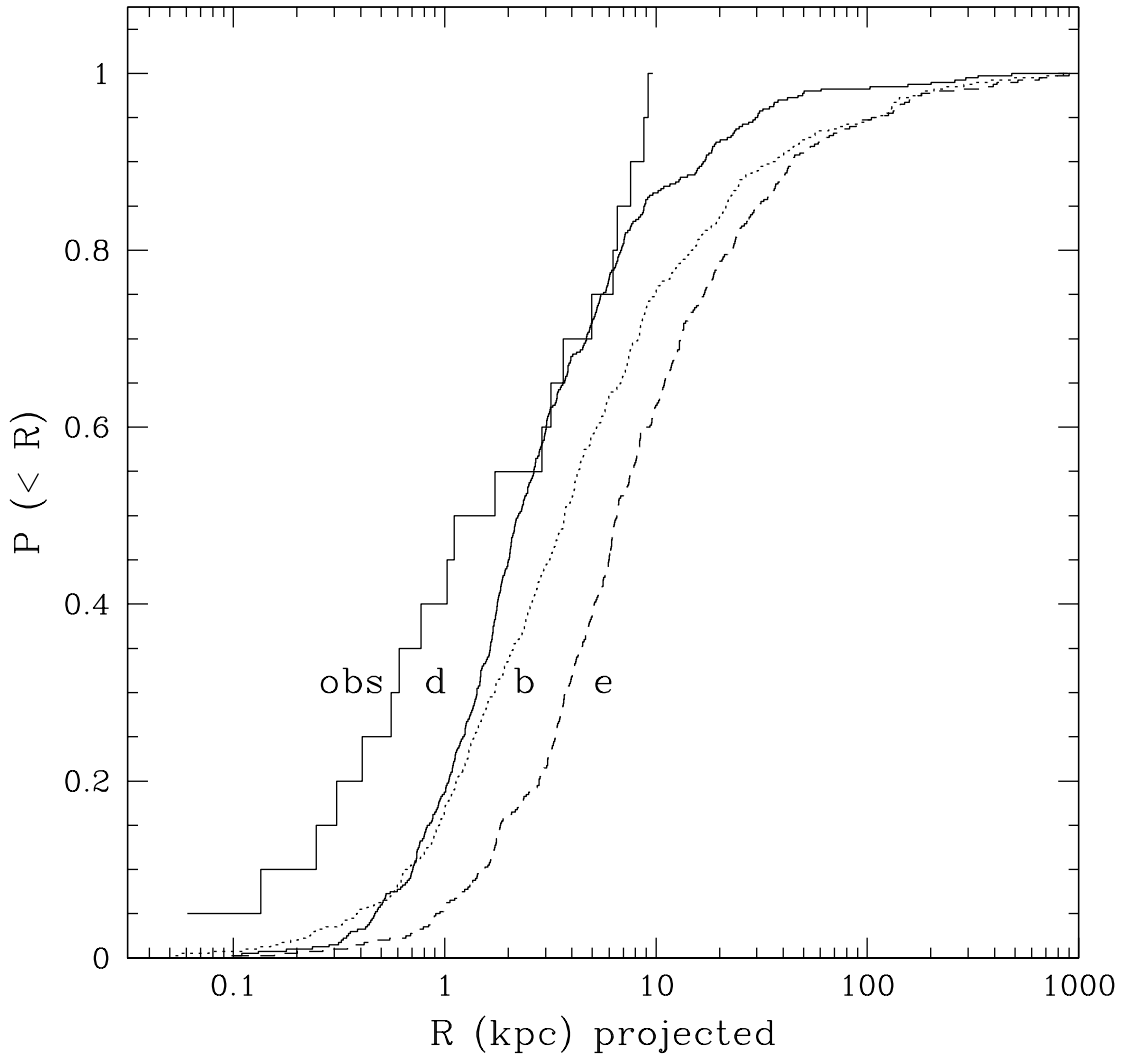


Figure 13. Distribution of the projected distances of the merger site from the galactic centre. This is shown for three galactic models: models d, b, and e (see Bloom et al. 1999 for a discussion of the galactic models). We also plot the observed distribution from Bloom et al. (2002) (square, solid line).